that some of the CH_4 on 1993SC exists in a solid solution with another component, perhaps N_2. Nevertheless, the precision and resolution of the existing data combined with the effects cited above make it difficult to reach that conclusion with any certainty.

In addition to the uncertainty introduced when using low-resolution spectral data, it is also unclear whether N_2 on 1993SC could be stable against long-term loss to space. A calculation of the temperature distribution on the surface of a body at a distance of 35 astronomical units from the sun, assuming a bolometric bond albedo of 0.05 and rotation period of 6 hours, gives a peak daytime temperature of 50 K at the equator of a spherical body with very low thermal inertia. At this temperature N_2 and CO have relatively high vapor pressures (4.0 and 0.88 mbar, respectively), but CH_4 ice has a much lower vapor pressure (3 μbar) (*18*). As such, it is unclear whether a body 300 km in diameter (*19*) has enough surface gravity to retain compounds like N_2 and CO over the age of the solar system. Thus, although it is reasonable to conclude that the spectrum of 1993SC is consistent with a CH_4-like hydrocarbon on its surface, making the leap to a CH_4-like hydrocarbon in solid solution with another, more volatile compound like N_2 is thermodynamically problematic.

The spectrum of 1993SC is also interesting because its reflectance increases by about a factor of 2 over the 1.4- to 2.4-μm region. This is much redder than the spectrum of Triton, but slightly less red than the slope of the average visual (0.4 to 0.8 μm) reflectance of 1993SC reported by Luu and Jewitt (*20*). Overall, the spectral slope of 1993SC could be due to complex organic molecules (*21*) on its surface, as well as simple hydrocarbons such as CH_4. Lastly, the similarity of the spectrum of 1993SC to that of Pluto (*22*) (Fig. 2) strengthens the case for CH_4 on 1993SC and appears at least to be consistent with the idea that Pluto and Triton may be the largest members of the population of bodies that made up the early Kuiper belt (*6*). Whether this spectral similarity is significant in light of the possibly very different evolutionary paths taken by Triton, Pluto, and 1993SC is unclear.

REFERENCES AND NOTES

1. G. P. Kuiper, in *Astrophysics: A Topical Symposium*, J. Hynek, Ed. (McGraw-Hill, New York, 1951), pp. 357–424.
2. K. E. Edgeworth, *Mon. Not. R. Astron. Soc.* **109**, 600 (1948)
3. J. H. Oort, *Bull. Astron. Inst. Neth.* **11**, 91 (1950).
4. M. Duncan, T. Quinn, S. Tremaine, *Astrophys. J. Lett.* **328**, L69 (1988).
5. D. Jewitt, J. Luu, J. Chen, *Astron. J.* **112**, 1225 (1996).
6. A. J. Cochran, H. F. Levinson, S. A. Stern, M. J. Duncan, *ibid.* **110**, 342 (1995).
7. Orbital elements were obtained from B. Marsden, Smithsonian Astrophysical Observatory (1996).
8. The program Ephem is marketed by Celestech, P.O. Box 61091, Honolulu, HI 96839, USA.
9. K_s is the K short filter whose passband encompasses the short-wavelength half of the standard K band.
10. The convolution to a lower resolution was done as a pure convolution. The effect of that convolution is to model how the data would look if obtained with an intrinsically lower resolution spectrometer. Application of our convolution technique to other data sets showed that no artifacts were introduced. The effect is simply one of a Fourier filter where the high frequencies in the transform of the data are attenuated by a Gaussian filter.
11. D. P. Cruikshank *et al.*, *Science* **261**, 742 (1993).
12. D. P. Cruikshank, T. C. Owen, C. deBergh, T. Geballe, unpublished data.
13. G. Herzberg, *Infrared and Raman Spectra of Polyatomic Molecules* (Van Nostrand, New York, 1945).
14. R. B. Bohn, S. A. Sandford, L. J. Allamandola, D. P. Cruikshank, *Icarus* **111**, 151 (1994).
15. B. Schmitt, E. Querico, S. Doute, T. Owen, C. deBergh, D. P. Cruikshank, paper presented at the 27th meeting of the Division of Planetary Sciences, American Astronomical Society, Kona, HI, 9 to 13 October 1995.
16. E. Quirico, thesis, Université Joseph Fournier, Grenoble, France (1996).
17. T. C. Owen *et al.*, *Science* **261**, 745 (1993).
18. G. N. Brown and W. T. Zeigler, *Adv. Cryog. Eng.* **25**, 662 (1979).
19. I. P. Williams, D. P. O'Ceallaigh, A. Fitzsimmons, B. G. Marsden, *Icarus* **116**, 180 (1995).
20. J. X. Luu and D. C. Jewitt, *Astron. J.* **111**, 499 (1994).
21. C. Sagan and B. Khare, *Nature* **227**, 102 (1979).
22. T. C. Owen, D. P. Cruikshank, C. deBergh, T. R. Geballe, unpublished data.

23. The W. M. Keck Observatory is operated as a scientific partnership between the California Institute of Technology and the University of California. It was made possible by the generous financial support of the W. M. Keck Foundation. We acknowledge the assistance of W. Harrison at the telescope. We dedicate this paper to the memory of Professor Carl Sagan whose scientific contributions have strongly influenced the concepts presented here.

14 February 1997; accepted 14 April 1997

Modeling of Cometary X-rays Caused by Solar Wind Minor Ions

Roman M. Häberli, Tamas I. Gombosi,* Darren L. De Zeeuw, Michael R. Combi, Kenneth G. Powell

X-ray emission was discovered in comet Hyakutake (C/1996 B2) by the Röntgen satellite in 1996, and these emissions were attributed to the excitation of high charge state solar wind ions due to electron capture from cometary molecules or atoms. Using the plasma flow in the coma of Hyakutake calculated by a three-dimensional adaptive magnetohydrodynamic model, the density distribution of solar wind ions in the coma and the resulting x-ray emission were computed. The calculated High Resolution Imager count rate of 4.4 per second and the spatial distribution of the x-ray emission agree with the observations. A detailed energy spectrum of cometary x-rays is predicted in the 80 to 2000 electronvolt energy range. Cometary x-rays present a sensitive tool to monitor cometary activity and solar wind ion composition.

Observations of comet C/1996 B2 (Hyakutake) by the Röntgen x-ray satellite (ROSAT) revealed the emission of soft x-rays from the coma at an unexpectedly high level of about 10^{25} photons s^{-1} (*1*). Of several possible explanations including fluorescent scattering of solar x-rays, interaction with interplanetary dust particles, and bremsstrahlung created by the cometary plasma, none satisfactorily explains the observed magnitude and shape of the emission (*1*). The observed x-ray emission may be caused by charge exchange excitations (CXE) of high charge state solar wind ions (O^{7+}, O^{6+}, C^{6+}, and others) with neutral molecules or atoms in the comet (*2*). Reactions such as $O^{7+} + H \rightarrow O^{6+*} + H^{+}$ occur in the upper atmosphere of Jupiter due to interaction with the solar wind, and an analogous mechanism may explain cometary x-rays (*3*). The electron is most likely captured into an excited state of the solar wind minor ion (*4*), leading to emission of soft x-ray and extreme ultraviolet (EUV) radiation. This process is efficient and often used as a diagnostic tool to monitor low-atomic number (Z) elements in laboratory plasmas (*5*).

Using a three-dimensional (3D) single-fluid magnetohydrodynamic (MHD) model of cometary plasma environments (*6*) we calculated the solar wind velocity and streamlines in the coma. The model uses conservation of mass, momentum, and energy, as well as the induction equation to compute the plasma mass density, flow, and pressure and the magnetic field in the coma. Ionization of cometary gas, recombination of ions with electrons and ion-neutral collisions are taken into account as source terms. Adequate resolution in all parts of the coma is ensured by the use of

R. M. Häberli, T. I. Gombosi, D. L. De Zeeuw, M. R. Combi, Space Physics Research Laboratory, University of Michigan, Ann Arbor, MI 48109–2143, USA.
K. G. Powell, Department of Aerospace Engineering, University of Michigan, Ann Arbor, MI 48109–2143, USA.

To whom correspondence should be addressed. E-mail: tamas@umich.edu

adaptive mesh refinement (*7*). The computed ion flow in the coma of Hyakutake appropriate for the conditions on 27 March 1996 when the x-ray emissions were observed (*1*) was obtained with a total gas production rate of 2.4×10^{29} s^{-1} (*8, 9*) (Fig. 1).

The densities of the major heavy ($Z > 2$) solar wind ions (Table 1) are computed by integrating the coupled system of continuity equations along the streamlines using the vector flow field from the MHD calculation. The production or loss of a particular species by charge exchange with cometary gas is taken into account as source terms to the equations. We include charge exchange with the cometary species H, O, H_2O, OH, and CO to calculate the cascading from high to low charge states. For the O and C ions, the velocity-dependent charge exchange cross sections with H and H_2 in the velocity range from 5.0×10^6 to 1.0×10^8 cm s^{-1} were measured (*10*). We used the H–cross sections for H and O and the H_2–cross section for H_2O, OH, and CO. This might be an underestimation because charge exchange cross sections generally tend to be larger for heavier molecules (*11*), however, we do not expect deviations greater than 20 to 30%. For charge exchange of the Ne ions with the neutral species we estimate a constant cross section of 4.0×10^{-15} cm^2. This falls right into the range of observed cross sections (*4*). A near constant cross section for energies below 10 keV amu^{-1} is also a reasonable assumption (*5*). To calculate the densities of the neutral species we used a modified Haser model (*12*) which allows for neutral outflow speeds varying with species and distance according to the results of a kinetic model (*13*).

In the case of CXE of a fully stripped ion X^{q+} with an atom or molecule of similar ionization potential as H, the excited state population of the $X^{(q-1)+}$ ion will be peaked around $n = q^{0.75}$ (14), where q is the atomic number and n is the charge state. The distribution of excited states is narrow at low energy (less than a few kiloelectron volts per atomic mass unit) but broadens at energies above 10 keV amu^{-1} (*15*). Because the energy of relative motion in our case will be at or below 1 keV amu^{-1}, we assumed that all electrons get captured into a shell with $n \simeq q^{0.75}$. We assume the same behavior for partially stripped ions, in this case, n is increased by 1 if the lowest shell is already occupied by electrons. For intermediate n levels, the excitation takes place into the highest angular momentum state (*5*). Based on atomic selection rules, the de-excitation takes place primarily in transitions of $\Delta n = 1$ (*5*). Calculations show that $\Delta n = 1$ transitions are more probable than $\Delta n = 2$ transitions by a factor of 5 to 10 at x-ray and EUV wavelengths (*5*). We therefore assumed that the de-excitation of the excited ions occurs only in steps of $\Delta n = 1$. Because most of the lines above an energy of 80 eV (Table 2) which can be expected from the ion species (Table 1) occur from the second lowest shell into the lowest possible shell, the above assumptions are justified.

Using the calculated densities of the solar wind ions in the coma, we computed the

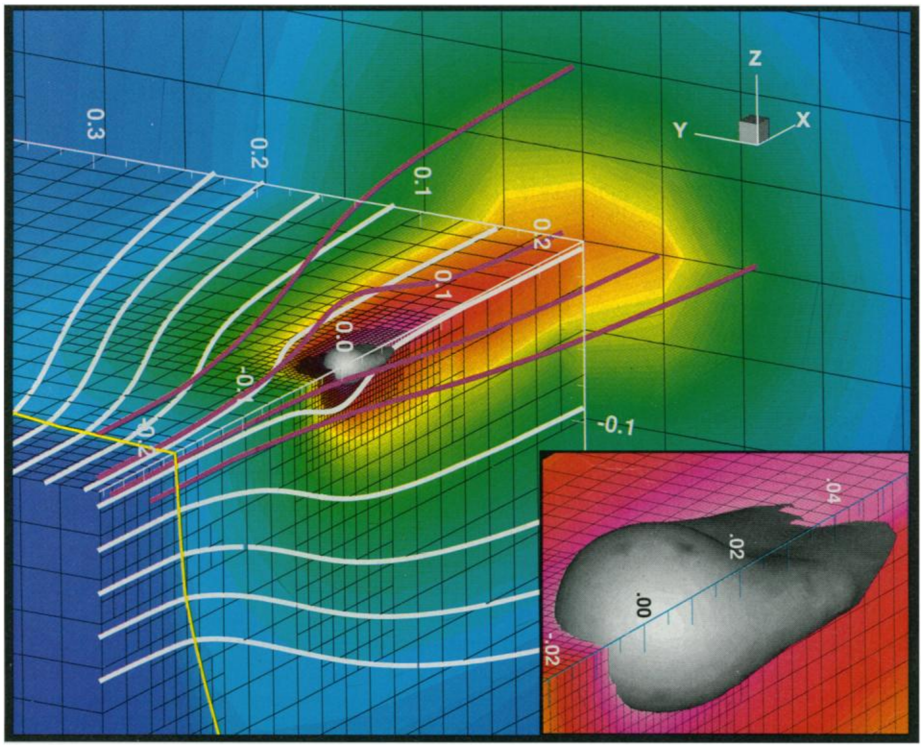

Fig. 1. Plasma flow field in the coma of Hyakutake on 27 March 1996, as computed by the 3D MHD model (*6*). Solar wind streamlines originating from the sun, which is to the left in the figure, are shown as white and purple lines. The yellow line shows the location of the bowshock. Color code gives logarithm of plasma mass density, increasing from blue to red. The bulb in the center of the figure (also on the inset) shows a surface of constant plasma mass density. Scales are given in 10^6 km.

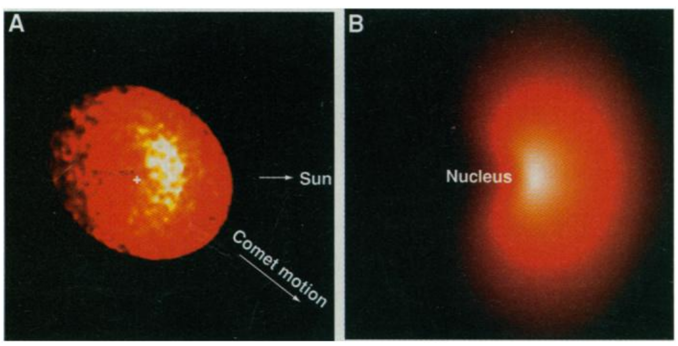

Fig. 2. Image (**A**) of the x-ray emission from Hyakutake, measured by the ROSAT HRI on 27 March 1996 (*1*). Computed image (**B**) of sum of all emission lines in the HRI passband (*1, 16*) caused by the charge exchange of solar wind ions with cometary gas. In both images, the x-ray emission shows a crescent shape and the maximum of the emission is displaced sunward from the nucleus. The scale of both images is the same.

Table 1. List of ions in our model of charge exchange excitation.

Ion	Upstream density* (cm^{-3})
O^{7+}	1.1×10^{-3}†
O^{6+}	2.07×10^{-3}†
O^{5+}	0.0‡
O^{4+}	0.0‡
O^{3+}	0.0‡
C^{6+}	8.8×10^{-4}†
C^{5+}	4.8×10^{-4}†
C^{4+}	0.0‡
C^{3+}	0.0‡
Ne^{8+}	3.7×10^{-4}†
Ne^{7+}	0.0‡
Ne^{6+}	0.0‡
Ne^{5+}	0.0‡
Ne^{4+}	0.0‡

*Proton density = 6.0 cm^{-3} (*9*). †Elemental abundances from (*18*). Charge state distributions from (*23*). ‡Produced by cascading from higher charge states.

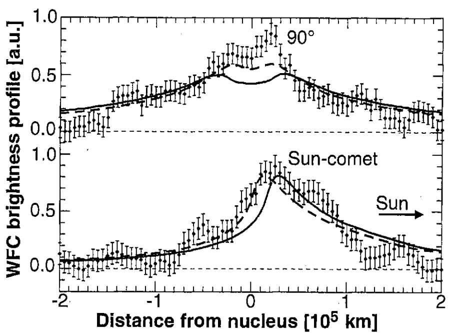

Fig. 3. Measured (diamonds) and computed (solid line) profile of x-ray intensity for the WFC (*1*, *16*). The computed results have been scaled to the same integrated brightness as the measurements from 27.8 March 1996 (*1*). The dashed lines show the computed profiles when the position of the nucleus is shifted sunward by 15,000 km (≃ resolution of WFC). We assumed that the measurement error is 10% of the peak value which approximately corresponds to the noise level in the observations. (**Top**) Shows the profile perpendicular to the sun-comet line and (**Bottom**) shows the profile along the sun-comet line. The direction of the sun in noted by the arrow.

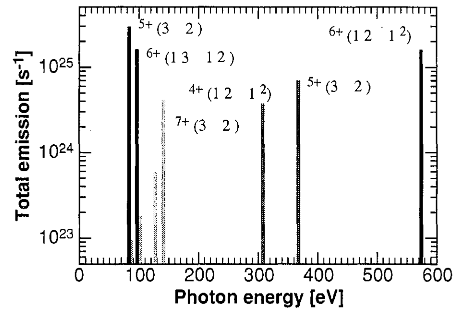

Fig. 4. Calculated x-ray energy spectrum in the 80-eV to 2-keV range. We note that the spectrum is fairly universal and is expected to change only moderately from comet to comet. The location of the spectral lines and their intensity is primarily controlled by the solar wind ion composition.

rate of CXE for every species and the corresponding volume emission rate of photons. By integrating the volume emission rate along the line-of-sight for 27.0 March universal time (UT) and summing over a field-of-view of $(4 \times 10^5\ \mathrm{km})^2$, centered around the nucleus, we obtained the total photon emission rates in Table 2. The total calculated count rate for the High Resolution Imager (HRI) is 4.42 s^{-1} (*16*), which agrees with the measured count rate of the slowly varying emission of 3.14 to 8.93 s^{-1} (*1*). The calculated Wide Field Camera (WFC) count rate is 0.278 s^{-1}, compared with a measured sporadic emission between 0.080 and 0.174 s^{-1} (*1*). Due to the uncertainties involved with the modeling (*17*), we claim success in explaining the observed x-ray radiation if the computed luminosity agrees with the measured one within a factor of 2; this clearly is the case for the HRI. The WFC count rate is dominated by emission from Ne^{7+} (Table 2). Therefore, the overestimation of the WFC count rate might be caused by an overestimate of the Ne/O ratio in the solar wind, which is uncertain by ±35% (*18*). In addition, we may have overestimated the charge exchange cross sections for Ne ions.

The calculated spatial distribution of the sum of all lines for the HRI (*1*, *16*) has a crescent-like shape with the maximum displaced from the nucleus by about 35,000 km along the sun-comet line, in agreement with the 27 March (*1*, *19*) HRI observations (Fig. 2). The crescent shape is caused by the depletion of solar wind ions due to charge exchange with cometary molecules and ions when approaching the comet. The computed x-ray brightness for the WFC (*16*) along the sun-comet line and at 90° to the sun-comet line is similar to the measured WFC brightness (*1*) (Fig. 3). The computed signal has been scaled to the same integrated brightness as the measured brightness, which was given in arbitrary units (*1*). Although the measured image (Fig. 2) shows that there is little emission from the nucleus, this is not clear in the profile at 90°. The lower spatial resolution of the WFC might cause the position of the nucleus to be uncertain. We have therefore displaced the nucleus sunward by 15,000 km (which is about the WFC resolution) in the computed image to demonstrate the sensitivity of the result on the nucleus position (Fig. 3).

Using the strength of our 3D MHD model, we computed the intensity and the spatial distribution of cometary x-rays created by CXE of heavy solar wind ions as proposed by Cravens (*2*). The results are in agreement with the observed total luminosity and shape of the slowly varying observed x-ray emission from Hyakutake (*1*). The calculation predicts the detailed energy spectrum which has not been observed yet (Fig. 4 and Table 2). Unlike other proposed mechanisms, which depend on unknown parameters [such as the size distribution of attogram particles (*20*), the level of electromagnetic wave activity (*21*), or energetic electron fluxes (*22*)] the CXE mechanism depends only on known physical properties of the solar wind and the cometary coma and plasma. The presence of heavy, high charge state ions in the solar wind has been established by in situ measurements (*18*) and the effectiveness of CXE is known from laboratory measurements (*5*).

The appearances and relative intensities of individual spectral lines of cometary x-ray emission are primarily controlled by the composition of the solar wind. The CXE generation of cometary x-rays represents a potentially powerful tool to monitor not only cometary activity far from Earth, but also the composition and flux of the solar wind. By measuring the detailed energy spectrum of cometary x-rays we might be able to monitor the quiet time solar wind as well as the propagation of coronal mass ejections and other transient interplanetary phenomena throughout the inner heliosphere.

Table 2. List of expected lines above 80 eV and the total emissions due to the CXE of solar wind ions. The wavelength of the transition is taken from (*24*). Calculated count rates are for a geocentric distance of 0.127 AU, accounting for the energy-dependent sensitivity (*16*).

Ion	Transition	Wavelength (Å)	Energy (eV)	Emission (10^{24} s^{-1})	HRI (s^{-1})	WFC (s^{-1})
O^{6+}	($1s2p$-$1s^2$)	21.60	574.0	16.1	2.722	0
O^{6+}	($1s3d$-$1s2p$)	128.5	96.49	16.1	0.312	0.0660
O^{5+}	($3p$-$2s$)	150.1	82.60	25.9	0.320	0.0543
C^{5+}	($2p$-$1s$)	33.74	367.5	6.10	0.636	0
C^{4+}	($1s2p$-$1s^2$)	40.27	307.9	3.75	0.095	0
Ne^{7+}	($3p$-$2s$)	88.09	140.7	4.16	0.300	0.1366
Ne^{6+}	($2s3p$-$2s^2$)	97.5	127.2	0.589	0.029	0.0183
Ne^{5+}	($3d$-$2p$)	122.5	101.2	0.180	0.004	0.0025
Ne^{4+}	($2p3d$-$2p^2$)	142.5	87.01	0.096	0.001	0.0004

REFERENCES AND NOTES

1. C. M. Lisse *et al.*, *Science* **274**, 205 (1996).
2. T. E. Cravens, *Geophys. Res. Lett.* **24**, 105 (1997).
3. H. J. Waite Jr. *et al.*, *J. Geophys. Res.* **99**, 14799 (1994); T. E. Cravens, E. Howell, J. H. Waite Jr., G. R. Gladstone, *ibid.* **100**, 17153 (1995).
4. R. Mann, F. Folkmann, H. F. Beyer, *J. Phys. B At. Mol. Phys.* **14**, 1161 (1981); D. Dijkkamp, Yu. S. Gordeev, A. Brazuk, A. G. Drentie, F. J. de Heer, *ibid.* **18**, 737 (1985).
5. R. C. Isler, *Plasma Phys. Control. Fusion* **36**, 171 (1994).
6. T. I. Gombosi, D. L. De Zeeuw, R. M. Häberli, K. G. Powell, *J. Geophys. Res.* **101**, 15233 (1996). This model is able to reproduce the bulk plasma parameters measured in situ at comet P/Halley and the ground-based observations of H_2O^+ [R. M. Häberli, M. R. Combi, T. I. Gombosi, D. L. De Zeeuw, K. G. Powell, *Bull. Am. Astron. Soc.* **28**, 1085 (1996)].
7. D. De Zeeuw and K. G. Powell, *J. Comp. Phys.* **104**, 56 (1993).
8. H_2O production on 24.5 March UT was 1.7×10^{29} s^{-1} [M. J. Mumma *et al.*, *Science* **272**, 1310 (1996)], 2.4×10^{29} s^{-1} on 3.5 April UT [M. R. Combi *et al.*, *Bull. Am. Astron. Soc.* **28**, 1094 (1996)]. Interpolated to 1.9×10^{29} s^{-1} on 27.0 March UT. We assumed

that H_2O accounts for 80% of the total gas production [D. Krankowsky *et al.*, *Nature* **321**, 326 (1986)].
9. The solar wind conditions in the models were obtained from WIND satellite data (http://web.mit.edu/afs/athena/orgls/space/www.html), interpolated for 27.0 March UT since WIND was in the magnetosheath. The solar wind parameters used in the simulation were: speed = 470 km/s, number density = 6 cm^{-3}, solar wind temperature = 8.8×10^4 K, magnetic field components B_x = 4.5 nT, B_y = −2.0 nT, B_z = 0 nT.
10. R. A. Phaneuf, I. Alvarez, F. W. Meyer, D. H. Crandall, *Phys. Rev. A* **26**, 1892 (1982).
11. H. Tawara, *At. Data Nucl. Data Tables* **22**, 491 (1978).
12. L. Haser, *Bull. Acad. R. Belg. Classes Sci. Ser. 5* **43**, 740 (1957).
13. M. R. Combi, *Icarus* **123**, 207 (1996).
14. R. E. Olson, *J. Phys. B At. Mol. Opt. Phys.* **13**, 483 (1980).
15. R. E. Olson and D. R. Schultz, *Phys. Scripta T* **28**, 71 (1989).
16. The expected count rates for the ROSAT instruments have been calculated for a geocentric distance of 0.127 AU using the energy-dependent effective area of the instruments as published in the ROSAT user's manual (http://ftp.rosat.mpe-garching/mpg.de/). The degradation of the WFC sensitivity with time after launch has been taken into account.
17. The solar wind composition and charge state distribution of ions vary considerably with time [for example, R. von Steiger, S. P. Christon, G. Gloeckler, F. M. Ipavich, *Astrophys. J.* **389**, 791 (1992)]. CXE cross sections have errors of 20 to 30%. The measured gas production rate and solar wind parameters have errors of 10 to 20%. Other ions, such as N, Si, and F, have not yet been included.
18. The O/H ratios are from S. J. Bame, J. R. Asbridge, W. C. Feldman, M. D. Montgomery, and P. D. Kearney [*Sol. Phys.* **43**, 463 (1975)]. The C/O ratios are from (23). The Ne/O ratios are from J. Geiss, R. von Steiger, G. Gloeckler, and A. B. Galvin [*Eos* **75** (no. 16), 278 (1994)].
19. C. Lisse *et al.*, http://www.astro.umd.edu/~lisse/rosat.html.
20. R. Bingham, J. M. Dawson, V. D. Shapiro, D. A. Mendis, B. J. Kellett, *Science* **275**, 49 (1996).
21. V. A. Krasnopolsky, *Bull. Am. Astron. Soc.* **28**, 1095 (1996).
22. T. G. Northrop, C. M. Lisse, M. J. Mumma, M. D. Desch, *Icarus*, in press.
23. P. Bochsler, J. Geiss, S. Kunz, *Sol. Phys.* **103**, 177 (1986).
24. R. L. Kelly and L. J. Palumbo, *Atomic and Ionic Emission Lines Below 2000 Angstroms* (Naval Research Laboratory, Washington, DC, 1973).
25. This work was supported by NASA under grants NAGW-1907, NAGW-1366, and NCCS5-146 and by NSF under grants AS7-9618795 and ATM-9318181. R.M.H. acknowledges partial support by the Swiss National Science Foundation. We thank T. E. Cravens for helpful discussions.

4 March 1997; accepted 17 April 1997

A Proficient Enzyme Revisited: The Predicted Mechanism for Orotidine Monophosphate Decarboxylase

Jeehiun K. Lee and K. N. Houk

A mechanism is proposed to explain the activity of orotidine 5′-monophosphate decarboxylase (ODCase). This enzyme is the one of the most proficient known, with a catalytic proficiency $(k_{cat}/K_m)/k_{non} = 10^{23}\ M^{-1}$. Quantum mechanical calculations predict a mechanism involving a stabilized carbene intermediate, which represents a previously unrecognized mode of enzymatic activity for ODCase. The proposed mechanism involves proton transfer from a weak acid (pK_a = 7, where K_a is the acid constant) concerted with decarboxylation, in a nonpolar enzyme environment. Such a mechanism makes possible different approaches to the design of ODCase inhibitors. Furthermore, the prediction that general acid catalysis may only be effective in low dielectric media is of general significance for understanding the activity of many enzymes.

The decarboxylation of orotidine 5′-monophosphate (OMP) (Fig. 1, **1a**; all bold numbers here refer to labeled structures in Fig. 1) to form uridine 5′-monophosphate (UMP, **2a**) by orotidine 5′-monophosphate decarboxylase (ODCase) is an essential step in nucleic acid biosynthesis (*1*). In bacteria and fungi, ODCase exists alone as a separate protein, whereas in mammals the ODCase activity is part of a bifunctional protein, UMP synthase (*2*). The conversion of **1** to **2** is also biomechanistically unique, in that all other biochemical decarboxylations involve stabilization of the carbanion intermediate by delocalization of the electron pair into a π orbital (*3*, *4*). For the decarboxylation of **1**, however, no such stabilization is present; a nonconjugated carbanion is formed. ODCase is one of the most proficient enzymes known (*1*). Proficiency is the second-order rate constant for the enzymatic reaction divided by the nonenzymatic rate constant $[(k_{cat}/K_m/k_{non})]$. For ODCase, the proficiencey is 2.0×10^{23} M^{-1}. The catalytic efficiency (k_{cat}/K_M) of ODCase, as with many enzymes, is nearly diffusion-controlled (*1*); it is the excruciating slowness of the uncatalyzed decarboxylation ($k_{non} = 2.8 \times 10^{-16}\ s^{-1}$) that produces the high proficiency.

The mechanism by which ODCase effects the efficient decarboxylation has long been a subject of interest among chemists and biochemists but remains unknown (*1*, *5*). The lack of any detectable cofactors or metal ions makes this mechanistic problem even more intriguing (*6*–*9*). Although no crystal structure of ODCase exists (*10*, *11*), it has been shown that 6-azauridylate (**3a**) and barbituric acid ribonucleotide (**4a**) are particularly prodigious inhibitors of yeast ODCase [inhibition constant $(K_I) = 5.1 \times 10^{-7}$ and 8.8×10^{-12} M, respectively] (*5*, *8*). Studies by Jones *et al.* of the enzyme mechanism indicate that Lys^{93} is important for catalysis but not for binding (*12*). In addition, the ratio of the maximal catalytic rate V_{max} to K_M of ODCase is pH-dependent, with a maximum at pH 7; this result has been interpreted to indicate that the enzyme possesses a catalytic group that has a pK_a of ~7 (*7*, *12*). Recently, catalytic antibodies have been developed to catalyze the decarboxylation of orotate (*9*, *13*).

Various mechanistic hypotheses have been proposed to explain the enormous rate enhancement by ODCase. Silverman *et al.* suggested a covalent mechanism involving nucleophilic attack at C-5, but this was subsequently shown by ^{13}C and D isotope effects to be unlikely (*6*, *7*, *14*). Beak *et al.* examined the decarboxylation of 1,3-dimethylorotic acid in sulfolane and proposed that decarboxylation occurred via zwitterion (**5**) (*5*). The fast (4×10^8 acceleration over the parent reaction) decarboxylation of betaine (**6**) led the authors to propose that the enzyme might effect catalysis by favoring formation of zwitterion (**5**). This mechanism has long been widely accepted (*6*–*9*, *15*). The protonation of the weakly basic orotate to form the zwitterion, however, seems unlikely.

An enzyme as proficient as ODCase is expected to be unusually "sensitive to . . . reversible inhibitors [that are] designed to resemble the [transition structure]" (*1*). The biological and medicinal importance of this reaction is clear: As a key biosynthetic step, the decarboxylation is a natural target for antitumor agents and genetic diseases such as orotic aciduria. Knowledge of the transition structure facilitates inhibitor design; herein, calculations are used to predict a transition state for this biologically and medicinally important reaction.

The energetics of the decarboxylation were explored by full optimizations of geometries and reaction paths along the decarboxylation reaction coordinate with the use of restricted Hartree-Fock (RHF) calculations with the 6-31+G* basis set. Energetics were obtained by single-point sec-

Department of Chemistry and Biochemistry, University of California, Los Angeles, CA 90095, USA.